Artificial Intelligence In Medicine 108 (2020) 101919

Contents lists available at ScienceDirect

Artificial Intelligence In Medicine

journal homepage: www.elsevier.com/locate/artmed

Continuous blood pressure measurement from one-channel electrocardiogram signal using deep-learning techniques

Fen Miao[a,1], Bo Wen[a,1], Zhejing Hu[a], Giancarlo Fortino[b], Xi-Ping Wang[d], Zeng-Ding Liu[a], Min Tang[e,**], Ye Li[a,c,*]

[a] Key Laboratory for Health Informatics of the Chinese Academy of Sciences, Shenzhen Institutes of advanced technology, Shenzhen, China
[b] Department of Informatics, Modeling, Electronics and Systems, University of Calabria, 87036 Rende CS, Italy
[c] Joint Engineering Research Center for Health Big Data Intelligent Analysis Technology, Shenzhen Institutes of Advanced Technology, Chinese Academy of Sciences. Shenzhen, Guangdong 518055, China
[d] Xinjiang Shihezi People's Hospital, Xinjiang 832000, China
[e] Fuwai Hospital, Chinese Academy of Medical Sciences, Beijing 100037, China

ARTICLE INFO

Keywords:
Blood pressure
Residual network
Long short-term memory
ECG

ABSTRACT

Continuous blood pressure (BP) measurement is crucial for reliable and timely hypertension detection. State-of-the-art continuous BP measurement methods based on pulse transit time or multiple parameters require simultaneous electrocardiogram (ECG) and photoplethysmogram (PPG) signals. Compared with PPG signals, ECG signals are easy to collect using wearable devices. This study examined a novel continuous BP estimation approach using one-channel ECG signals for unobtrusive BP monitoring. A BP model is developed based on the fusion of a residual network and long short-term memory to obtain the spatial-temporal information of ECG signals. The public multiparameter intelligent monitoring waveform database, which contains ECG, PPG, and invasive BP data of patients in intensive care units, is used to develop and verify the model. Experimental results demonstrated that the proposed approach exhibited an estimation error of 0.07 ± 7.77 mmHg for mean arterial pressure (MAP) and 0.01 ± 6.29 for diastolic BP (DBP), which comply with the Association for the Advancement of Medical Instrumentation standard. According to the British Hypertension Society standards, the results achieved grade A for MAP and DBP estimation and grade B for systolic BP (SBP) estimation. Furthermore, we verified the model with an independent dataset for arrhythmia patients. The experimental results exhibited an estimation error of −0.22 ± 5.82 mmHg, −0.57 ± 4.39 mmHg, and −0.75 ± 5.62 mmHg for SBP, MAP, and DBP measurements, respectively. These results indicate the feasibility of estimating BP by using a one-channel ECG signal, thus enabling continuous BP measurement for ubiquitous health care applications.

1. Introduction

As the leading cause of death worldwide, cardiovascular diseases (CVDs) were estimated to account for 17.7 million deaths in 2017 [1]. Hypertension is the greatest risk factor for CVDs and should thus be detected as early as possible [1]. Unfortunately, the prevalence of hypertension continually rises due to population aging and low awareness and treatment rates [2,3]. Reliable and timely blood pressure (BP) measurement is imperative for the prevention of hypertension and related CVDs. Systems for monitoring risk factors, such as BP and heart rate, related to heart health have been shown to provide indispensable support in the prevention and diagnosis of CVDs [4,5]. Although BP can be measured at clinics using auscultation and oscillometric techniques, certain conditions, such as “masked” hypertension and “white-coat”

Abbreviation: BP, Blood pressure; CVD, Cardiovascular disease; PTT, Pulse transit time; ECG, Electrocardiogram; PPG, Photoplethysmogram; SBP, Systolic blood pressure; MAP, Mean arterial pressure; DBP, Diastolic blood pressure; CNN, Convolutional neural network; RNN, Recurrent neural network; ResNet, Residual network; LSTM, Long-short term memory network; MIMICIII, Multi-parameter Intelligent Monitoring in Intensive Care III; AAMI, Association for the Advancement of Medical Instrumentation; BHS, British Hypertension Society; MD, Mean difference; MAD, Mean absolute difference; STD, Standard deviation of the difference

* Corresponding author at: Key Laboratory for Health Informatics of the Chinese Academy of Sciences, Shenzhen Institutes of advanced technology. Shenzhen, China.
** Corresponding author.
E-mail addresses: doctortangmin@hotmail.com (M. Tang), ye.li@siat.ac.cn (Y. Li).
[1] Authors contributed equally.

https://doi.org/10.1016/j.artmed.2020.101919
Received 26 September 2019; Received in revised form 24 June 2020; Accepted 24 June 2020
Available online 27 June 2020
0933-3657/

hypertension cannot be effectively identified in clinical examination; yet, both are strongly associated with increased CVD risk [6]. The prevalence of masked hypertension is also high—between 8% and 20%—and can be up to 50% in hypertensive patients receiving treatment [7]. Continuous or ambulatory BP is recommended to identify these patients [4]. However, traditional ambulatory BP-monitoring devices commonly use an oscillometric technique that requires a cuff to be repeatedly inflated around the arm. Such devices cause discomfort and even pain for the user, especially during sleep, and thus limit its appropriate usage during routine health care. Therefore, demand for cuffless devices that can provide continuous BP monitoring unobtrusively and ubiquitously is increasing [8].

Several cuffless BP methods have been proposed that are based on electrocardiogram (ECG) and photoplethysmogram (PPG), including pulse transit time (PTT) and multiparameter-based approaches [9–25]. PTT refers to the time taken for a pulse wave to propagate between two locations in the cardiovascular system and can be calculated from two pulse signals generated by the cardiovascular system, such as ECG and PPG. As an extensively studied method for cuffless BP measurement, PTT-related approaches [9–17] require two channels of physiological signals [18]. Multiparameter-based approaches [18–26] have subsequently been proposed for improving the PTT-based models by merging various parameters extracted from ECG and PPG signals that influence BP. These approaches have exhibited superior performance. Machine learning algorithms such as support vector machine, random forest, and neural networks have been used in such approaches to develop BP models based on ECG and PPG signals [26]. However, most multiparameter-based models require two channels of physiological signals, and models based on one-channel PPG signal exhibit inferior performance [19]. Compared with PPG signals, ECG signals are easier to implement in a wearable item, such as a T-shirt or wristwatch [27,28]. Using one-channel ECG signals to estimate BP is a suitable method for monitoring continuous BP unobtrusively and ubiquitously in routine health care applications.

Deep learning techniques can discover deep features without any handcrafted engineering and have been proved to be a powerful tool for image classification problems [29,30]. Deep learning methods are also being increasingly used to solve medical problems and even to process physiological signals [31–33]. Su et al. proposed a long short-term memory network (LSTM)-based model to evaluate continuous BP using ECG and PPG signals, and experimental results suggested it significantly improved long-term BP estimation accuracy [34]. The application of deep learning techniques for discovering deep-level features of ECG signals, and estimating BP could be a potential approach for achieving continuous BP measurement.

This study examined a novel concept for continuous BP estimation using an approach based on ECG signals. The main contributions of this paper are as follows: (1) The proposed model estimates BP with only one-channel ECG signals, enabling continuous BP measurement with wearable devices. (2) This is the first study to fuse a convolutional neural network (CNN) and LSTM to capture both morphological and rhythmic features of ECG signals without any handcrafted engineering to generate high-accuracy BP estimates. (3) Performance was validated using numerous patients from an intensive care unit (ICU) and an independent hospital database for patients with arrhythmia, indicating good reliability.

The rest of the paper is organized as follows. The proposed methodology is described in Section II. Experimental results are provided in Section III, and a discussion on the implications of the proposed approach is presented in Section IV. Section V concludes the paper.

2. Background

2.1. Related research on the relationship between BP and ECG

Generally speaking, three factors, including cardiac contractility, blood volume, and peripheral resistance, are responsible for BP variation. State-of-the-art research has demonstrated that ECG signals can be used to evaluate cardiac contractility [35], and ECG might reasonably be assumed to exhibit a close relationship with BP variation. Until now, few papers have researched the relationship between BP and ECG signals [36–40]. Ahmad et al. and Chan et al. [36,37] have conducted studies on the relationship between ECG and BP, but both relied on additional sensors such as PPG sensors. Researchers have also discussed the relationship between ECG signals and BP, but the only information they used from ECG signals was heart rate and RR intervals, and they confirmed that there was no strong relationship between morphological changes in ECG signals and BP changes [38,39]. Simjanoska et al. [40] input ECG signals to estimate BP, but they used a simple combination of traditional machine learning models, such as a support vector machine and linear regression model, and a limited dataset of 51 participants.

2.2. Residual network

As a popular structure in deep learning, a CNN consists of the use of a series of convolutional layers, nonlinear layers, and downsampling layers to capture the patterns of input data from the global receptive field. With increasing network depth, the accuracy of a CNN increases. Whereas, when the network depth increases to a certain level, the accuracy decreases rapidly as the deeper network becomes more difficult to optimize. The residual network (ResNet) [41] approach is an outstanding means of implementing a CNN. ResNet solves the problem of degraded CNN performance in extremely deep conditions with a simple structure, and its short connection structure breaks the traditional layer-by-layer transmission of neural networks; consequently, the output of the previous layer can directly jump several layers to be the input of a later layer. The structure of ResNet can accelerate the training of ultra-deep neural networks, yielding improved accuracy.

2.3. LSTM

LSTM, proposed by Hochreiter and Schmidhuber in 1997, is an artificial recurrent neural network (RNN) architecture with feedback connections [42]. LSTMs are explicitly designed to avoid long-term dependency problems. LSTMs have chain-like structures, and four interacting neural network layers comprise the repeating module. An LSTM module typically has a memory cell, input gate, output gate, and a forget gate in addition to the hidden state in traditional RNNs. It has recently been applied to detect heart disease because ECG signals contain repeated heartbeat information that is closely related to time in 2019 [33]. LSTMs exhibit superior performance in processing entire sequences of data to capture time-related features.

3. Methodology

In this study, we propose a deep learning architecture called Res-LSTM for continuous BP estimation. The proposed Res-LSTM contains a 50-layer ResNet and a bidirectional LSTM [43] model. A block diagram of the proposed approach for continuous BP estimation is presented in Fig. 1. First, a preprocessing procedure that includes noise filtering, signal segmentation, and normalization is implemented for the original ECG signals. Because ECG is a sequential signal, a ResNet and a bidirectional LSTM are combined to capture both morphological and rhythmic features from preprocessed signals that may influence BP variation. Next, two fully connected layers follow for concatenation of the aforementioned features for estimation. The output from the fully connected layer is combined with the baseline BP for each experimental participant in a regression model to generate the final continuous BP.

3.1. Clinical database

In this study, two datasets are used to develop and verify the BP

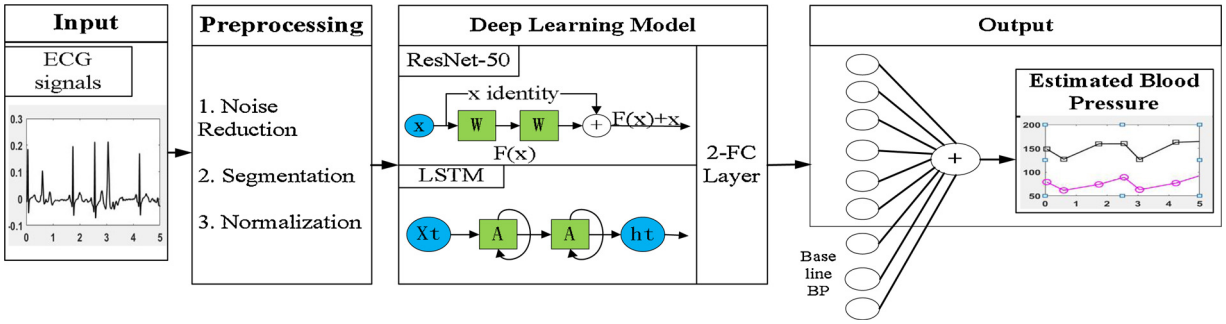

Fig. 1. Block diagram of the proposed model.

model, including the public multiparameter intelligent monitoring (MIMIC III) waveform database [44,45] for ICU patients and a database of patients with cardiac arrhythmias (ARR database) collected from Fuwai Hospital, Chinese Academy of Medical Sciences.

The MIMIC III database contains physiological signals and time series of vital signs captured from ICU patients. All data were collected from a variety of ICUs (medical, surgical, coronary care, and neonatal) in a single tertiary teaching hospital between 2001 and 2008. The dataset consists of multiple channels of physiological signals (ECG, PPG, arterial BP) and time series of vital signs (heart rate, systolic BP [SBP], diastolic BP [DBP]) for 5599 patients. The sampling rate of the physiological signals is 125 Hz. Notably, some recordings are not ideal for analysis and modeling because of missing or noisy data, and so some preprocessing methods are used that are explicated in the next subsection. A total of 897 743 heartbeats of physiological signals from 1711 patients remain in the final dataset, and the statistics of the BP distribution are shown in Table 1.

ARR database information was collected from 30 adult patients with cardiac arrhythmias, including atrial fibrillation, ventricular premature beat, and ventricular tachycardia. Data were collected at Fuwai Hospital, Chinese Academy of Medical Sciences. Patients were excluded if they were unable to provide informed consent or had a difference in SBP or DBP between the cuff-based measurements on their two upper arms > 5 mmHg. A monitoring system (Mindray N12, Shenzhen, China) was used to acquire synchronous ECG, PPG, and invasive arterial BP signals for each patient in the supine position before the radiofrequency ablation procedure. The sample rate for ECG, PPG, and arterial BP collection was set to 125 Hz. The dataset contains 1342 beats of physiological signals from 30 patients after preprocessing, and the BP distributions are shown in Table 2. BP values in the ARR database are observed to have the same distribution as those in the MIMIC III database. This study was approved by the Ethics Committee of Fuwai Hospital, Chinese Academy of Medical Sciences.

3.2. Data preprocessing

We first implement preprocessing procedures for the ECG signal, including noise filtering, signal segmentation, and normalization.

Noise filtering: A noise filtering method is implemented in this study to remove noise from original ECG signals. ECG signals are first preprocessed using a low-pass filter with a cutoff frequency of 50 Hz to remove high-frequency interference, and the baseline drift of ECG is

Table 1
Summary of the Study Population BP Distributions from the MIMIC III Database.

	Min (mmHg)	Max (mmHg)	STD (mmHg)	Mean (mmHg)
SBP	80.01	180.00	20.57	135.69
MAP	66.79	126.55	10.78	93.04
DBP	60.00	100.00	8.84	71.72

Table 2
. BP Distributions in the Arrhythmia Database.

	Min (mmHg)	Max (mmHg)	STD (mmHg)	Mean (mmHg)
SBP	105.15	179.94	19.54	137.07
MAP	81.84	119.67	10.83	97.97
DBP	60.07	92.11	8.17	73.42

then removed with wavelet transformation [17]. A nine-level wavelet decomposition is performed with the order 8 Daubechies (db8) wavelet. The coarse scale approximation coefficients (CA) and the detail coefficients (CD) are extracted. CA of the first level, which represents the low-frequency baseline wandering, and CDs of the seventh to ninth levels, which represent some high-frequency disturbance, are replaced by zeros. After reconstruction of the signal based on the decomposition coefficients, ECG signals free of baseline wandering are obtained.

Signal segmentation: ECG signals are first segmented into multiple heartbeats according to the R-waves of ECG signals, with each ECG signal representing a heartbeat corresponding to an SBP–DBP pair extracted from the simultaneous arterial BP waveform. To reduce the signal variation, a set of three heartbeats is combined to correspond to one SBP–DBP value pair, which is the mean value of the extracted SBP–DBP values of the three heartbeats. The question is that the lengths of ECG signals differ for different heartbeat cycles due to heart rate variations. Because ResNet and LSTM both require input data of the same length, cropping or padding techniques are thus applied to the ECG signal to fix the input data length. More specifically, if the length of the ECG signal exceeds the fixed length, the corresponding ECG signal is cropped to match the fixed length randomly. Otherwise, the corresponding ECG signal is padded with zeros at both ends. According to the statistics, the average heartbeat cycle for ICU patients and patients with arrhythmia is approximately 0.8 s. Thus, we crop and pad each ECG signal segment into a fixed length of 300 points, which generally encompasses three heartbeats for further modeling.

Normalization: ECG signals for different individuals vary widely in amplitude, and this affects the model performance significantly. A data normalization method is therefore used, and the function is defined as:

$$Normalized(X^i) = \frac{X^i - \overline{X}}{S^i} \tag{1}$$

where X^i refers to the input ECG signal, $\overline{X}$ refers to the mean value of X^i, and S^i refers to the standard deviation of X^i.

Formally, the new signal after data preprocessing is $X_{new} = \mathrm{Pre}(X)$, where Pre(.) stands for a series of data preprocessing steps, X is the original dataset, and X_{new} is a new dataset transformed from the original dataset. Here, $X_{new} = \{X^1_{new}, X^2_{new}, ..., X^i_{new}\}$ and $X^i_{new} = (x_1, x_2, ..., x_l)$, where $l = 300$.

The SBP and DBP values for estimation are extracted from the arterial BP waveform. SBP value is defined as the peak value of the arterial BP waveform; the DBP value is the average of the bottom values for each heartbeat. The ECG signals and corresponding BPs are

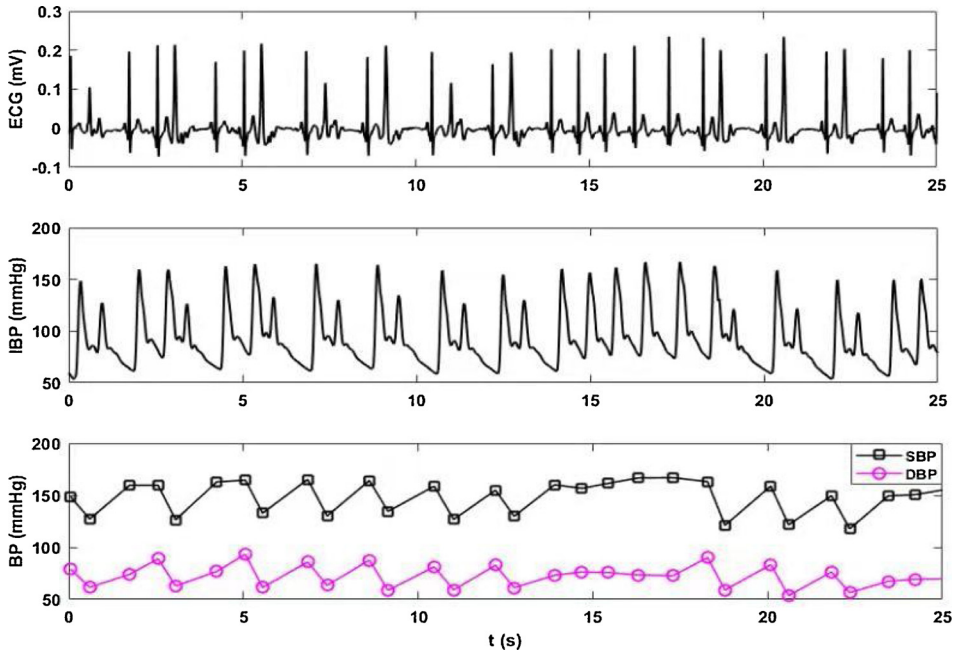

Fig. 2. Typical example of the input ECG signal, corresponding BP waveform, and SBP–DBP values.

presented in Fig. 2.

3.3. Proposed deep learning architecture

First, a 50-layer ResNet is employed here for morphological ECG feature extraction. It is used in this study to capture influential but tiny features in ECG signals. The architecture of the proposed 50-layer ResNet is similar to that of the original framework described in [41]. The original ResNet is used for pixel-based image classification, whereas this paper addresses sequential signals, and thus some modifications are applied to fit ECG signals to learn small features of ECG signals, such as P, R, Q, S, T, and U waves. The greatest difference between image classification and ECG signals is that ECG signals are always one dimensional with repeated heartbeat patterns; thus, the larger kernel size of 9 is implemented for dimension reduction instead of the kernel size of 3 originally used in ResNet. The number of filters is set as 16, 32, 64, and 128 instead of 64, 128, 256, and 512, respectively. Therefore, 128 small features are learned through the use of ResNet. Finally, 128 features are concatenated together for further modeling. Formally, given a preprocessed signal X^i_{new}, the features of a 50-layer residual network are $R^i = \text{Res50}(X^i_{new})$, where Res50(.) represents a series of procedures in ResNet and feature concatenation of 128 small features.

The LSTM model is often used to capture time-related features because it can memorize useful information from previous time steps. A time-related model, such as LSTM, is therefore a reasonable choice for application to ECG signals, enabling morphological features from ResNet to be supplemented with time-related features from the LSTM model. The LSTM-model input is the preprocessed ECG signal X^i_{new}, and the output is defined as $L^i = \text{LSTM}(X^i_{new})$, where LSTM(.) is the LSTM-model procedure. In addition, the LSTM model is known to require a series of time-related data inputs, so X^i_{new} is reshaped to a new vector $X^j_{lstm} = (x^i_{lstm,1}, x^i_{lstm,2}, \ldots, x^i_{lstm,t})$ and $x^i_{lstm,t} = (x_1, x_2, \ldots, xl_1)$, where $t, l_1 \in N$ and $t \times l_1 = l$.

Finally, the concatenation of R^i, L^i from ResNet and LSTM further serves as input in this step and connects to two fully connected layers, $\hat{y}^i = f(f([R^i, L^i]))$, where $[x, y]$ indicates the concatenation of x and y, and $f(.)$ represents a fully connected layer that linearly transforms inputs and is then activated by a predefined nonlinear transformation. Here, $\hat{y}^i$ is the final feature extracted for SBP and DBP estimation. To overcome individual specificity and thus improve estimation accuracy, the baseline BP for each experimental participant is combined with the final features to estimate continuous SBP and DBP. Specifically, a vector of three features of personal BP information is implemented as baseline BP $C^i = (C^i_{high}, C^i_{mean}, C^i_{low})$, where C^i_{high} is the highest BP of person $i$during one particular time period (2 min in our study), C^i_{mean} is the average BP of person i in that particular time period, and C^i_{low} is the lowest BP in that time period. The proposed model then concatenates $\hat{y}^i$ and C^i and outputs $\hat{y}^i_C$. Formally, $\hat{y}^i_C = \vec{a} \cdot [\hat{y}^i, C^i] + b$, where $\vec{a}$ and b are learned parameters. Overall, the result of the proposed approach is $\hat{y}^i_C$.

3.4. Implemental detail and analysis

3.4.1. Training, validation and test dataset

A total of 1711 individuals remain in the MIMIC III dataset, and recordings number 897743 after preprocessing. The preprocessed MIMIC III dataset is then randomly split into training, validation and test datasets. Sixty-five percent of patients from the preprocessed MIMIC III dataset are chosen to use to train the model, which contains 1112 patients with 583,533 recordings. Ten percent of patients are chosen as the validation dataset to derive the parameters of the model. The remaining data from 428 patients are used for testing the performance of the BP model. In addition, the independent ARR database is also used to test the BP model, which contains 1342 recordings from 30 different patients after preprocessing. We label a new sample according to the heartbeat cycle: three heartbeat cycles are used for BP estimation.

3.4.2. Experimental environment

The proposed model runs on the deep learning framework pytorch 0.4.1, using the ubuntu 16.04.1 LTS operating system. The computing server is equipped with eight NVIDIA Tesla TITAN Xp, four 30 multiprocessors (total: 15 360 cores), and 12 GB memory (total: 48 GB memory). In addition, the platform running pytorch is deployed on the high-performance computing server equipped with two 24-core Intel Xeon E5-2650 V4 processors with 128 GB memory.

The NumPy v1.13 library of Python is used mainly for implementation of the code. We perform data analysis using the scikit-learn 0.21 library.

3.4.3. Hyperparameters

For the modified ResNet50, the kernel size is set to 9 for dimension reduction instead of 3, as in the original ResNet; the numbers of filters are set to 16, 32, 64, and 128. The two-layer LSTM net contains 64 hidden neurons in each layer. To train the model, the batch size is set at 2048 to fill the memory of a single graphical processing unit (GPU). The number of time series t is set to 10. The learning rate is 0.0005 to balance the training speed and precision.

4. Experimental results

4.1. Accuracy performance

Four measurements, including total Pearson's correlation coefficient (r), total mean difference (MD), total mean absolute difference (MAD), and total standard deviation of mean difference (STD) are evaluated in this paper to measure the accuracy of the proposed model. In detail, $r$measures the consistency between the predicted value and the true value from a mathematical perspective, MD measures the error between the predicted value and the true value, MAD measures the absolute error between the predicted value and the true value, and STD measures the variation of MD. Formulas for these four measurements are as follows:

$$r = \frac{\sum_{i=1}^{n}(x_i - \bar{x})(y_i - \bar{y})}{\sqrt{\sum_{i=1}^{n}(x_i - \bar{x})^2}\sqrt{\sum_{i=1}^{n}(y_i - \bar{y})^2}} \tag{2}$$

$$MD = \frac{\sum_{i=1}^{n}(y_i - x_i)}{n} \tag{3}$$

$$MAD = \frac{\sum_{i=1}^{n}|y_i - x_i|}{n} \tag{4}$$

$$STD = \sqrt{\frac{\sum_{i=1}^{n}(y_i - x_i - MD)^2}{n-1}} \tag{5}$$

where x_i is the reference value of BP from the arterial BP, y_i is the predicted value of BP from the model, and n is the total number of values in the test dataset.

4.1.1. MIMIC III database

With the proposed Res-LSTM model, the Pearson's correlation coefficient r for overall estimated SBP, mean arterial pressure (MAP), and DBP for the MIMIC III database is 0.88, 0.85, and 0.71, respectively. The MD ± STD for SBP, MAP, and DBP estimates are -0.11 ± 9.99, -0.03 ± 6.66, and $0.01 \pm \pm 6.29$ mmHg, respectively. In addition, the MAD for SBP, MAP, and DBP is 7.10, 4.66, and 4.61. The correlation and Bland–Altman plots are shown in Fig. 3. In the correlation plots, the x-axis is the reference BP value, and the y-axis is the estimated BP value. Most points are observed to lie close to the line, suggesting a close correlation. In the Bland–Altman plot, the x-axis of the plots represents the average BP, defined as the mean of the estimation and the actual value; the y-axis represents the difference between the actual value and the estimated value. The bias (MD) and the limits of agreement (bias ± 1.96 × STD) are also illustrated in black dash dot lines. More than 95% of the points lie within the limit of agreement in SBP, DBP, and MAP evaluation, indicating the high estimation accuracies for SBP, DBP, and MAP achieved with the proposed method.

An evaluation of the proposed model based on the Advancement of Medical Instrumentation (AAMI) [46] standard is presented in Table 3. The AAMI standard requires the MD and STD of the measured BP value to be lower than 5 and 8 mmHg, respectively. As evident in the table, the proposed method achieves low MD values that approach 0 for SBP, MAP, and DBP. The proposed model achieves a total STD of 9.99 for SBP, which is slightly higher than the AAMI standard. The STDs of DBP and MAP both satisfy the AAMI standards, which indicates good DBP and MAP estimation performance. The evaluation of the proposed model based on British Hypertension Society (BHS) standards [47] is presented in Table 4. BHS standards measure the absolute error between reference BP and predicted BP for 5, 10, and 15 mmHg, respectively. The proposed method achieves grade B level for SBP. The values for 5, 10, and 15 mmHg conditions are 50.07%, 76.40%, and 90.39%, respectively. In addition, the model achieves a much higher according to BHS standards, of DBP and MAP evaluations that satisfy grade A. For DBP estimation, the proportions for 5, 10, and 15 mmHg are 65.14%, 89.58%, and 96.61%, respectively. For MAP estimation, the proportions for 5, 10, and 15 mmHg are 65.66%, 89.77%, and 96.62%, respectively.

4.1.2. ARR database

The proposed model is also tested on the independent ARR database to verify model performance. Table 5 presents the overall MAD, MD, and STD evaluation for SBP, MAP and DBP estimation. In terms of MD ± STD, the model achieves an overall accuracy of -0.22 ± 5.82 mmHg for SBP, -0.57 ± 4.39 for MAP, and -0.75 ± 5.62 for DBP, all of which satisfy the AAMI standards. In addition, MAD values for SBP, MAP, and DBP are 4.41, 3.56, and 4.37, respectively. The correlation and Bland–Altman plots are shown in Fig. 4. In the correlation plots, the correlation coefficients for SBP, MAP, and DBP estimations are observed to be 0.96, 0.91, and 0.74, respectively. The Bland–Altman plot also indicates high estimation accuracy levels for SBP, MAP, and DBP on the ARR database. In addition, the model is consistent with the grade A level—according to BHS standards—in the estimation of SBP, MAP, and DBP, and the result is presented in Table 6. The performance is clearly superior in the ARR database in the MIMIC III dataset. The main reason for this is that the ARR database captures a fixed scenario in which no patients were subjected to external stimulation that might have influenced BP variation; for example, the use of vascular drugs. In addition, the patients have the same types of diseases. However, in the MIMIC III database, the patients have various diseases and are subject to multiple stimulations, resulting in greater uncertainty in BP

4.2. Comparison with other machine learning methods and other studies

Table 7 presents a comparison of the proposed model and traditional machine learning or deep learning algorithms, including random forest, Adaboost, decision tree, linear regression, ResNet, and LSTM. All traditional algorithms are trained with default parameters, and all hyperparameters in deep learning models—including number of filters in each layer, kernel size, and number of paddings—are set to be the same as for the proposed model to enable comparison. Table 8 demonstrates that deep learning models outperform all traditional algorithms in terms of MAD and STD. Random forest outperforms all other traditional models in both SBP and DBP estimation, but it satisfies neither AAMI nor BHS standards. Overall, deep learning models are better able to estimate blood pressure than traditional algorithms because of their ability to recognize deep features with numerous parameters.

Moreover, the proposed Res-LSTM model outperforms ResNet and bidirectional LSTM only in terms of r, MD, MAD, and STD, implying that the combined model more effectively identifies deep features than ResNet or bidirectional LSTM models do alone. In detail, comparted the best model in traditional models (ResNet-50), the correlation coefficient (r) was increased from 0.8 to 0.88 with the proposed Res-LSTM model for SBP estimation, while the MAD was decreased from 0.83 to 7.10. This is reasonable because LSTM is able to obtain time-related information, such as heart rate, directly relating to BP, and ResNet captures small features of ECG signals that cause BP variation. Therefore, a combination of the two models provides more information than a single model does.

To further evaluate the superiority of the proposed model, we also compare the performance of our study with previous studies. Another

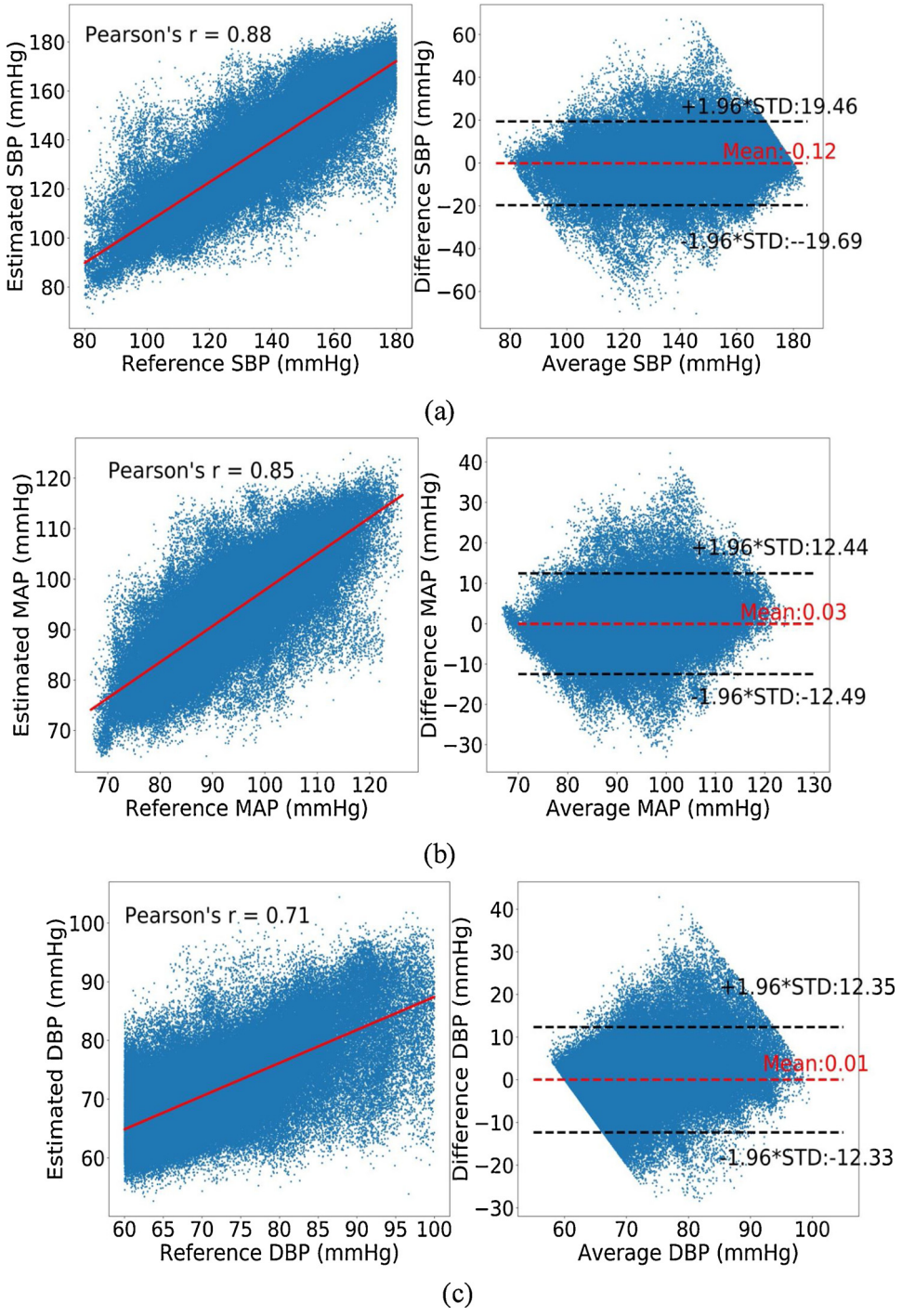

Fig. 3. Correlation and Bland–Altman plots of SBP, MAP, and DBP with reference arterial BP for MIMIC III database; (a) SBP (b) MAP (c) DBP.

Table 3
Accuracy Performance Evaluation Based on the AAMI Standard for the MIMIC III Database.

		MD (mmHg)	STD (mmHg)	Subjects
Our Results	SBP	−0.11	9.99	428
	MAP	−0.01	6.29	428
	DBP	−0.03	6.36	428
AAMI	SBP and DBP	≤5	≤8	≥85

Table 4
Accuracy Performance Evaluation Based on the BHS Standard for the MIMIC III Database.

		Cumulative Error Percentage		
		C.P. 5 mmHg	C.P. 10 mmHg	C.P. 15 mmHg
Our result	SBP	50.07 %	76.40 %	90.39 %
	MAP	65.14 %	89.58 %	96.61 %
	DBP	65.66 %	89.77 %	96.63 %
BHS	Grade A	60 %	85 %	95 %
	Grade B	50 %	75 %	90 %
	Grade C	40 %	65 %	80 %

Table 5
Accuracy Performance Evaluation Based on the AAMI Standard for the ARR Database.

		MD (mmHg)	STD (mmHg)	Subjects
Our Results	SBP	−0.22	5.82	30
	MAP	−0.57	4.39	30
	DBP	−0.75	5.62	30
AAMI	SBP and DBP	≤5	≤8	≥85

Table 6
Accuracy Performance Evaluation Based on the BHS Standard for the ARR Database.

		Cumulative Error Percentage		
		C.P. 5 mmHg	C.P. 10 mmHg	C.P. 15 mmHg
Our result	SBP	65.50 %	91.81 %	97.95 %
	MAP	76.02 %	97.37 %	99.42%
	DBP	70.76 %	92.69 %	97.96 %
BHS	Grade A	60 %	85 %	95 %
	Grade B	50 %	75 %	90 %
	Grade C	40 %	65 %	80 %

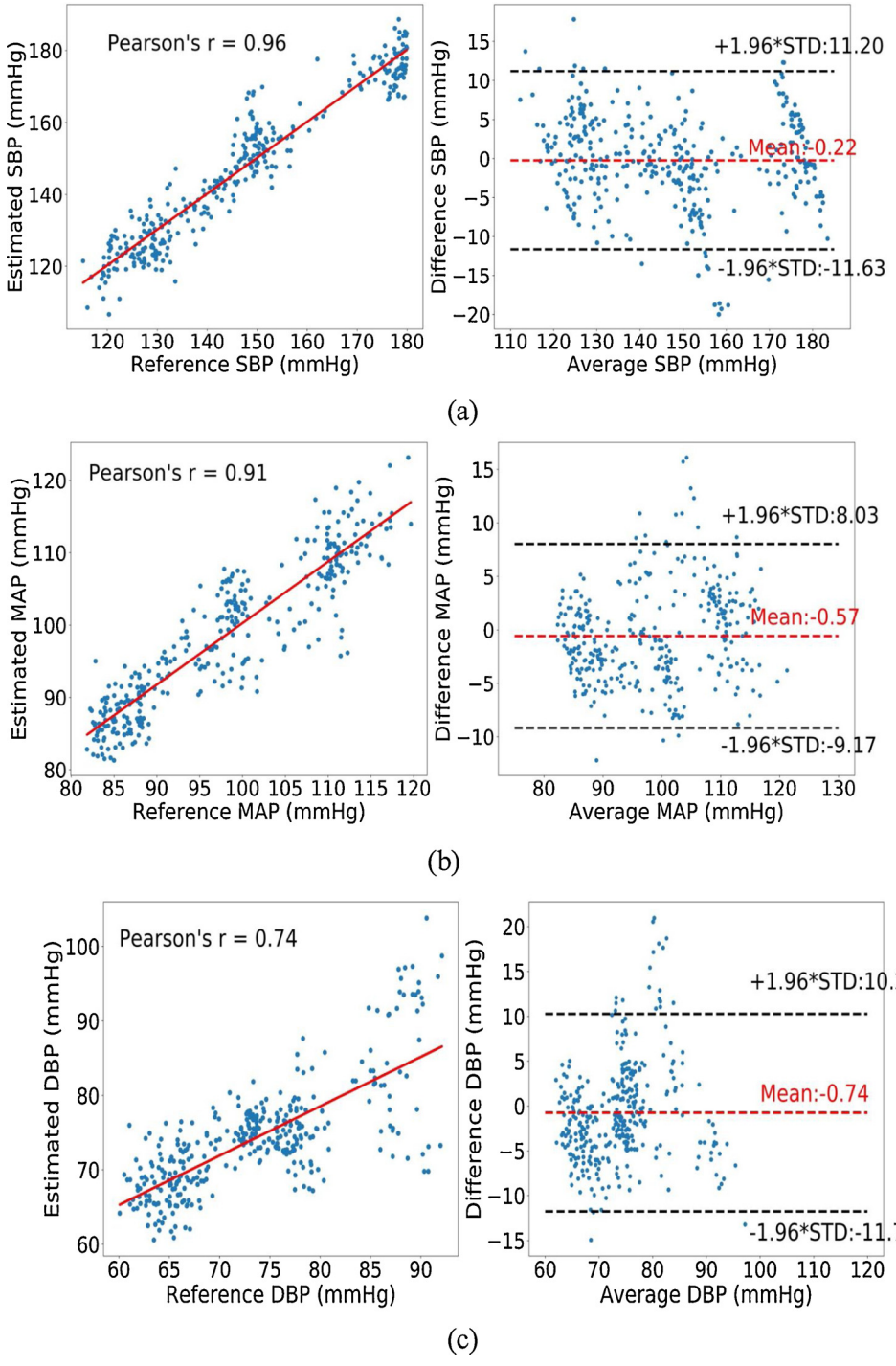

Fig. 4. Correlation and Bland–Altman plots of SBP, MAP, and DBP with reference arterial BP for arrhythmia database; (a) SBP (b) MAP (c) DBP.

Table 7
Comparison with Other Machine Learning algorithms.

	SBP				DBP			
	r	MD	MAD	STD	r	MD	MAD	STD
Linear Regression	0.34	22.76	42.02	22.41	0.68	10.21	21.48	16.18
Decision Tree	0.51	0.81	14.14	20.17	0.56	0.54	10.99	9.34
Random Forest	0.71	0.83	10.81	14.48	0.67	0.43	8.15	8.26
Adaboost	0.23	0.67	16.61	20.03	0.44	0.21	9.27	9.12
ResNet-50	0.82	0.01	8.32	11.87	0.71	−0.03	5.28	6.84
LSTM	0.8	0.89	9.10	13.1	0.67	0.52	6.31	8.07
Res-LSTM	0.88	−0.12	7.10	9.99	0.71	0.01	4.61	6.29

four studies are listed in Table 8 for comparison. It is thus apparent that the foremost advantage of the proposed model is that it relies only on the original ECG signals, enabling BP measurement with wearable devices. Although Simjanoska et al. proposed estimating BP using ECG signals [40], the proposed model notably outperforms their model for SBP, DBP and MAP evaluation with a larger dataset. Specifically, the MAD was decreased from 7.72 to 7.10 for SBP estimation, from 9.45 to 4.61 for DBP estimation and from 8.13 to 4.66 for MAP estimation. The number of this study's test dataset notably exceeds that in any other research, which implies that our results provide greater statistical reliability. Overall, our model achieves competitive accuracy, reliability, and ease of implementation.

4.3. Derivation of the hyperparameters

In the proposed Res-LSTM, hyperparameters, including the kernel size of ResNet and the number of time series of LSTM, were set to adapt the ECG signal processing. To verify the effectiveness of the values defined, we evaluated the accuracy performance on the validation dataset in terms of MAD with different kernel sizes and number of time series, as presented in Table 9. Kernel size of 3, 6, 9, and 12 and time series number of 10, 12, and 15 were implemented for comparison. The table indicated that the model with kernel size of 9 and time series number of 10 achieved the lowest MAD, exhibiting optimal performance. Therefore, 9 is selected as the kernel size of ResNet and 10 is selected as the number of time series of LSTM in our study.

4.4. Feature visualization

To further illustrate the reasons for the proposed combined model's superior performance compared with the single model's, we present the learned features from ResNet and LSTM, respectively. The learned features are mapped to the original signals through a deconvolution process, and the contribution of each segment in ECG signals to the final feature sets are presented with different gray levels. As presented in Fig. 5, the lower gray level indicates greater contribution. The figure indicates that ResNet is a powerful approach for identifying edge and small features, such as the QRS information of the first and last ECG signals in the three heartbeats. LSTM prioritizes the sequence features, which can reflect the timing information in ECG signals. Therefore, the combination of ResNet and LSTM achieves superior estimation accuracy.

Table 9
. Accuracy peformance of different hyperparameters in terms of mad for SBP estimation.

Kernel size / **No. of time series**	**3**	**6**	**9**	**12**
10	7.23	7.14	**7.08**	7.43
12	7.34	7.26	7.24	7.45
15	7.36	7.29	7.28	7.48

4.5. Computational complexity evaluation

The proposed model consists of three main parts, a ResNet, an LSTM network, and a fully connected network. The total number of parameters in the proposed model is 404 520, which requires a total memory of 1.54 MB. In terms of running speed, the proposed model converges after 500 epochs, and the training time of the proposed model for 500 epochs is approximately 995 min. In the testing phase, the test time for one single recording is approximately 50.58 ms, which means the proposed method is suitable for health care applications and provides feedback quickly. Table 10 compares the computational complexity of the proposed Res-LSTM and ResNet, LSTM algorithm only. Table 10 shows that the computational complexity of Res-LSTM is comparable to ResNet, greater than LSTM. However, considering superior accuracy performance achieved by Res-LSTM, we still choose it to develop the BP model in our study.

5. Discussion

5.1. Selection of number of layers in ResNet

The ResNet of 50 layers has been implemented in this paper for morphological feature learning. The number of layers N influences not only the accuracy but also the efficiency of the model. If too few layers are set, the model misses influential features; if too many are set, the learning speed is too slow, and this restricts its application in wearable devices. In this paper, N = 5, 18, 34, 50, and 128 are implemented for comparison, and the model performance values are listed in Table 11. As shown in Table 11, the model achieves the lowest MAD and STD when N = 50 and the highest correlation when N = 128. Moreover, the model with 128 layers performs the best in terms of BHS standards, and the model with 50 layers achieves similar results. Although the model performance is relatively similar when N = 50 and N = 128, the training time and complexity increase dramatically when N = 128. Therefore, N is fixed as 50 for the sake of the efficiency and accuracy of the model.

Table 8
Comparsion with Previous Studies.

	Signal Used	Dataset	SBP		DBP			MAP			
			MD	MAD	STD	MD	MAD	STD	MD	MAD	STD
This work	ECG	1711 ICU and 30 arrhythmia patients	−0.12	7.10	9.99	0.01	4.61	6.29	−0.03	4.66	6.36
[26]	ECG, PPG	57 ICU patients in MIMIC III	–	8.21	–	–	4.31	–	–	–	–
[21]	ECG,PPG	23 ICU patients in MIMIC III	–	8.7	–	–	4.6	–	–	4.4	–
[48]	PPG	172 subjects	−0.41	–	8.1	−1.53	–	6.4	–	–	–
[40]	ECG	51 subjects	–	7.72	10.22	–	9.45	10.03	–	8.13	8.84

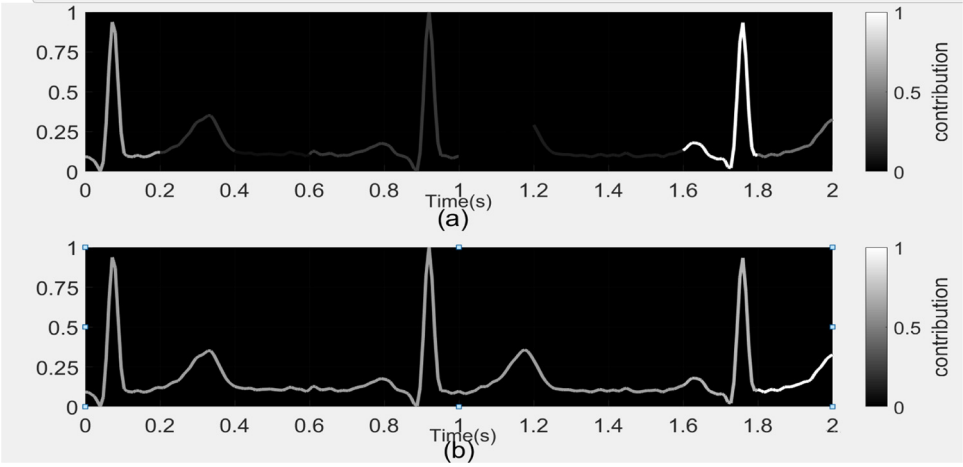

Fig. 5. Visualization of the features learned mapped to the original signal from ResNet and LSTM; (a) ResNet (b) LSTM.

Table 10
Computational Complexity Comparison for SBP Estimation.

	Number of parameters	Training time	Testing time
Res-LSTM	404,520	995m	87 ms
ResNet	258,242	916 m	75 ms
LSTM	148,874	232m	50 ms

Table 11
Accuracy of Different Numbers of Layers.

N		5	18	34	50	128
r		0.71	0.76	0.78	0.82	0.84
MD		0.26	0.05	0.02	0.01	−0.01
STD		12.97	12.74	12.81	11.85	11.87
MAD		10.34	9.42	9.03	8.29	8.32
BHS	< =5	41.15 %	44.63 %	45.87 %	46.13 %	46.18 %
	< =10	68.70 %	71.25 %	72.54 %	72.01%	72.48 %
	< =15	85.12 %	85.38 %	87.17 %	87.24 %	87.20 %

5.2. Evaluation of the proposed model for the tracking of individual BP changes

To evaluate the performance of the proposed model for tracking dynamic BP changes in individuals, Fig. 6 shows the estimated and reference SBP and DBP of one representative experimental participant from the MIMIC III test dataset. The *x*-axis is the number of beats and the y-axis is the BP value. Fig. 6 (a) and Fig. 6 (b) indicate that the proposed model is able to follow large variations in SBP and DBP precisely. Fig. 6 indicates that the proposed method has the ability to track major changes in BP for individuals, implying reliable performance.

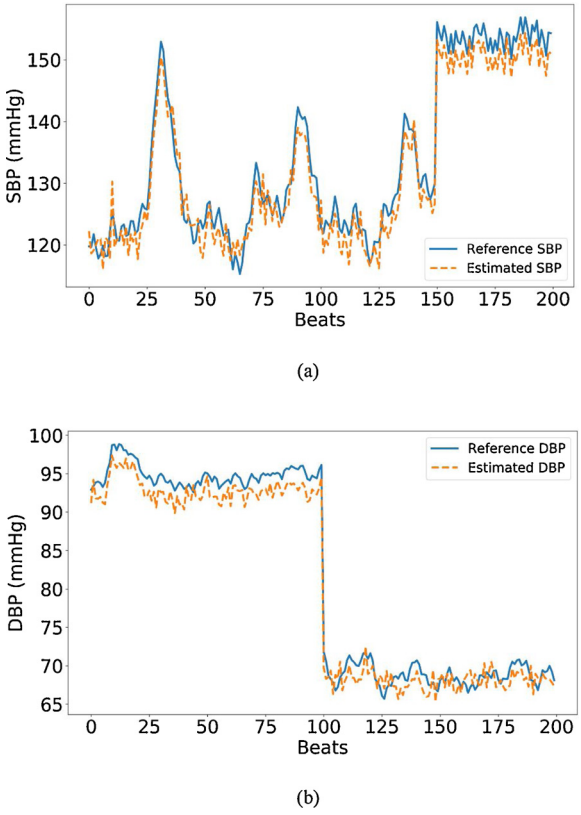

Fig. 6. Estimated beat-to-beat SBP and DBP with proposed method (green) and the reference (blue) of one representative experimental participant (For interpretation of the references to colour in this figure legend, the reader is referred to the web version of this article).

5.3. Limitations

Although the proposed approach demonstrated the feasibility of continuous BP monitoring using only a one-channel ECG signal, some uncertainties remain. First, multiple factors such as diseases, drugs, and individual differences may affect the BP variations, rendering the performance of the proposed approach uncertain. Therefore, the baseline BP for each experimental participant was used as an input variable in the BP model development process, and this can be adjusted to the individual factors. However, baseline BP works for only the same diseases and drug states, and it should be updated for other diseases and drugs. Therefore, further studies should be performed in the future on methods of updating the baseline BP through long-term monitoring of experimental participants. Second, the signals and reference BP values collected in clinical settings feature some noise, which influences the stability of the proposed model. Therefore, data preprocessing procedures were implemented before the model's development to reduce the noise and remove signals with poor quality.

6. Conclusions

This paper proposed a Res-LSTM framework for continuous BP estimation using only one-channel ECG signal, validating the model against two datasets. The Res-LSTM framework was based on the fusion of ResNet and LSTM to obtain the spatial-temporal information from the ECG signal. In the MIMIC III dataset, we achieved a grade B level

according to BHS standards for SBP estimation and a grade A level for DBP and MAP estimation. Furthermore, the model achieved a grade A level according to BHS standards for SBP, DBP, and MAP estimation, as verified through an independent test dataset from 30 individuals with arrhythmia, which implies the model demonstrated good feasibility and scalability. In comparison with other research, the proposed model offers competitive performance with only one-channel ECG signals. Overall, our research provides convincing evidence that ECG signals can be used for BP estimation, thus enabling continuous BP measurement in wearable devices for ubiquitous health care applications. In the future, demographic and clinical data, including age, sex, and diagnosed diseases will be considered in the model to expand its health care applicability.

Funding

This work was supported in part by the National Natural Science Foundation of China (No.61771465, U1913210), Shenzhen Science and Technology Projects (No. JCYJ20180703145202065) and Major Projects from General Logistics Department of People's Liberation Army (AWS13C008).

Declaration of Competing Interest

The authors declare no competing interests.

Appendix A. Supplementary data

Supplementary material related to this article can be found, in the online version, at doi:https://doi.org/10.1016/j.artmed.2020.101919.

References

[1] World health statistic 2018. Geneva, Switzerland: World Health Organization; 2018.
[2] Lackland Daniel T, Weber Michael A. Global burden of cardiovascular disease and stroke: hypertension at the core. Can J Cardiol 2015;31(May (5)):569–71.
[3] Lu J, Lu Y, Wang X, et al. Prevalence, awareness, treatment, and control of hypertension in China: data from 1Â·7 million adults in a population-based screening study (China PEACE Million Persons Project). Lancet 2017;390(10112):2549–58.
[4] Santos Marcus, Dos Alexandre G, et al. Online heart monitoring systems on the internet of health things environments: a survey, a reference model and an outlook. Inf Fusion 2020;53:222–39.
[5] De Moraes JL, Rocha MX, Vasconcelos G, et al. Advances in photopletysmography signal analysis for biomedical applications. Sensors 2018;18(6):1894–920.
[6] Ohkubo Takayoshi, Kikuya Masahiro, Metoki Hirohito, Asayama Kei, Obara Taku, Hashimoto Junichiro, et al. Prognosis of “masked” hypertension and “white-coat” hypertension detected by 24-h ambulatory blood pressure monitoring: 10-year follow-up from the Ohasama study. J Am Coll Cardiol 2005;46(3):508–15.
[7] Bobrie Guillaume, Clerson Pierre, Menard Joel, Postel-Vinay Nicolas, Chatellier Gilles, Plouin Pierre-Francois. Masked hypertension: a systematic review. J Hypertens 2008;26(9):1715–25.
[8] Zhang YT, Zheng YL, Lin WH, Zhang HY, Zhou XL. Challenges and opportunities in cardiovascular health informatics. IEEE Trans Biomed Eng 2013;60(March (3)):633–42.
[9] Ding XR, Zhao N, Yang GZ, Pettigrew R, Lo B, Miao F, et al. Continuous blood pressure measurement from invasive to unobtrusive: celebration of 200th birth anniversary of carl ludwig. IEEE J Biomed Health Inform 2016;20(6):1455–65.
[10] Mukkamala R, et al. Toward ubiquitous blood pressure monitoring via pulse transit time: theory and practice. IEEE Trans Biomed Eng 2015;62(August (8)):1879–901.
[11] Solà J, et al. Noninvasive and non-occlusive blood pressure estimation via a chest sensor. IEEE Trans Biomed Eng 2013;60(December (12)):3505–13.
[12] Huynh Toan Huu, Jafari Roozbeh, Chung Wan-Young. Noninvasive cuffless blood pressure estimation using pulse transit time and impedance plethysmography. IEEE Trans Biomed Eng 2018;66(4):967–76.
[13] Poon CCY, Zhang YT. Cuff-less and noninvasive measurements of arterial blood pressure by pulse transit time. 2005 IEEE Engineering in Medicine and Biology 27thAnnual Conference. 2005. p. 5877–80.
[14] Liu Q, Yan BP, Yu CM, Zhang YT, Poon CCY. Attenuation of systolic blood pressure and pulse transit time hysteresis during exercise and recovery in cardiovascular patients. IEEE Trans Biomed Eng 2014;61(February (2)):346–52.
[15] Zheng YL, Yan BP, Zhang YT, Poon CCY. An armband wearable device for overnight and cuff-less blood pressure measurement. IEEE Trans Biomed Eng 2014;61(July (7)):2179–86.
[16] Ding XR, Zhang YT, Liu J, Dai WX, Tsang HK. Continuous cuffless blood pressure estimation using pulse transit time and photoplethysmogram intensity ratio. IEEE Trans Biomed Eng 2016;63(May (5)):964–72.
[17] Ding XR, Zhang YT, Tsang HK. Impact of heart disease and calibration interval on accuracy of pulse transit time–based blood pressure estimation. Physiol Meas 2016;37:227–37. vol. 2.
[18] Miao F, Nan F, Zhang YT, et al. Novel continuous blood pressure estimation approach based on data mining techniques. IEEE J Biomed Health Inform 2017;21(6):1730–40.
[19] Lin WH, Wang H, Samuel OW, Liu G, Huang Z, Li GL. New photoplethysmogram indicators for improving cuffless and continuous blood pressure estimation accuracy. Physiol Meas 2018;39. vol. 2, Fed.
[20] Kachuee M, Kiani MM, Mohammadzade H, Shabany M. Cuffless blood pressure estimation algorithms for continuous health-care monitoring. IEEE Trans Biomed Eng 2017;64(April (4)):859–69.
[21] Yoon YZ, et al. Cuff-less blood pressure estimation using pulse waveform analysis and pulse arrival time. IEEE J Biomed Health Inform 2017.
[22] He X, Goubran RA, Liu XP. Secondary peak detection of PPG signal for continuous cuffless arterial blood pressure measurement. IEEE Trans Instrum Meas 2014;63(6):1431–9.
[23] He R, Huang ZP, Ji LY, Wu JK. Beat-to-beat ambulatory blood pressure estimation based on random forest. IEEE International Conference on Wearable and Implantable Body Sensor Networks. 2016. p. 194–8.
[24] Xu Z, Liu J, Chen X, Wang Y, Zhao Z. Continuous blood pressure estimation based on multiple parameters from eletrocardiogram and photoplethysmogram by back-propagation neural network. Comput Ind 2017;89(C):50–9. 2017.
[25] He DD, Winokur ES, Sodini CG. An ear-worn vital signs monitor. in IEEE Transactions on Biomedica Engineering 2015;62(November (11)):2547–52.
[26] Kachuee M, Kiani MM, Mohammadzade H, Shabany M. Cuffless blood pressure estimation algorithms for continuous health-care monitoring. IEEE Trans Biomed Eng 2017;64(April (4)):859–69.
[27] Nemati E, Deen MJ, Mondal T. A wireless wearable ECG sensor for long-term applications. Ieee Commun Mag 2012;50(1):36–43.
[28] Chan, H.L., Chao, P.K. and Jheng, J.C., Chang Gung University (CGU), "Device and method for measuring three-lead ECG in a wristwatch. " U.S. Patent 7,894,888.
[29] He K, Zhang X, Ren S, et al. Deep residual learning for image recognition[C]. in Proceedings of the IEEE Conference on Computer Vision and Pattern Recognition 2016:770–8.
[30] Wang Liwei, Li Yin, Lazebnik Svetlana. Learning deep structure-preserving image-text embeddings. IProceedings of the IEEE Conference on Computer Vision and Pattern Recognition 2016:5005–13.
[31] Hannun AY, Rajpurkar P, Haghpanahi M, Tison GH, Bourn C, Turakhia MP, et al. Cardiologist-level arrhythmia detection and classification in ambulatory electrocardiograms using a deep neural network. Nat Med 2019;25(1):65.
[32] Fan Xiaomao, Yao Qihang, Cai Yunpeng, Miao Fen, Sun Fangmin, Li Ye. Multiscaled fusion of deep convolutional neural networks for screening atrial fibrillation from single lead short ECG recordings. IEEE J Biomed Health Inform 2018;22(6):1744–53.
[33] Yao Q, Wang R, Fan X, et al. Multi-class Arrhythmia detection from 12-lead varied-length ECG using Attention-based Time-Incremental Convolutional Neural Network. Inf Fusion 2020:174–82.
[34] Su P, Ding X, Zhang Y, et al. Long-term blood pressure prediction with deep recurrent neural networks. Ieee EMBS International Conference on Biomedical and Health Informatics 2018:323–8.
[35] Attia Zachi I, Kapa Suraj, Lopez-Jimenez Francisco, McKie Paul M, Ladewig Dorothy J, Satam Gaurav, et al. Screening for cardiac contractile dysfunction using an artificial intelligence–enabled electrocardiogram. Nat Med 2019;25(1):70.
[36] Chan K, Hung K, Zhang Y. Noninvasive and cuffless measurements of blood pressure for telemedicine. In Proceedings of the 23rd Annual International Conference of the IEEE Engineering in Medicine and Biology Society. 2001. p. 3592–3. 25–28 October; Volume 4.
[37] Ahmad S, Chen S, Soueidan K, Batkin I, Bolic M, Dajani H, et al. Electrocardiogram-assisted blood pressure estimation. IEEE Trans Biomed Eng 2012;59:608–18.
[38] Schroeder EB, Liao D, Chambless LE, Prineas RJ, Evans GW, Heiss G. Hypertension, blood pressure, and heart rate variability. Hypertension 2003;42:1106–11.
[39] Hassan MKBA, Mashor M, Nasir NM, Mohamed S. Measuring of systolic blood pressure based on heart rate. In Proceedings of the 4th Kuala Lumpur International Conference on Biomedical Engineering. 2008. p. 595–8. 25–28 June.
[40] Simjanoska M, Gjoreski M, Gams M, et al. Non-invasive blood pressure estimation from ECG using machine learning techniques. Sensors 2018;18(4):1160.
[41] He K, Zhang X, Ren S, et al. Deep Residual Learning for Image Recognition. Computer vision and pattern recognition 2016:770–8.
[42] Hochreiter Sepp, Schmidhuber Jurgen. Long short-term memory. Neural Comput 1997;9(8):1735–80.
[43] Sak Haşim, Senior Andrew, Beaufays Françoise. Long short-term memory recurrent neural network architectures for large scale acoustic modeling. In Fifteenth Annual Conference of the International Speech Communication Association 2014.
[44] Johnson AEW, Pollard TJ, Shen L, Lehman L, Feng M, Ghassemi M, et al. MIMIC-III, a freely accessible critical care database. Sci Data 2016.
[45] Goldberger A.L., Amaral L.A.N., Glass L., Hausdorff J.M., Ivanov PCh, Mark R.G., Mietus J.E., Moody G.B., Peng C.-K., Stanley H.E. "PhysioBank, PhysioToolkit, and PhysioNet: Components of a New Research Resource for Complex Physiologic Signals," Circulation 101(23):e215-e220.
[46] American National Standard for Electronic or Automated Sphygmomanometers, ANSI/AAMISP102002,Arlington,VA,USA:Association for the Advancement Instrumentation, 2002.
[47] Brien EO, et al. The British Hypertension Society protocol for the evaluation of automated and semi-automated blood pressure measuring devices with special reference to ambulatory systems. J. Hypertension 1990;8(7):607–19.
[48] Watanabe Naoki, Bando Yasuko K, Kawachi Taiji, Yamakita Hiroshi, Futatsuyama Kouki, Honda Yoshikazu, et al. Development and validation of a novel cuff-less blood pressure monitoring device. JACC Basic Transl Sci 2017;2(6):631–42.